COMPUTATIONAL SUPPORT OF THE X-29A ADVANCED TECHNOLOGY DEMONSTRATOR FLIGHT EXPERIMENT

E. G. Waggoner
NASA Langley Research Center
Hampton, Virginia

B. L. Bates
Vigyan Research Associates, Inc.
Hampton, Virginia

INTRODUCTION

The X-29A Advanced Technology Demonstrator, figure 1, has been designed and developed to demonstrate the advantages of forward wing sweep along with other advanced technologies. Grumman Aerospace Corporation designed and fabricated the flight vehicle under a contract sponsored by the Defense Advanced Research Projects Agency and managed by the Air Force. A number of advanced technologies have been incorporated into the design. These include, in addition to the obvious forward-swept wing, a closely coupled canard, thin supercritical wing sections, discrete variable camber, aeroelastic tailoring, three-surface control, relaxed static stability, and a triple-channel digital flight control system.

An extensive flight-test program has been defined and is under way at NASA Ames/Dryden Flight Research Facility to acquire high-quality data which will be used to evaluate and correlate the original design analyses and ground-test results with flight results. One of the objectives of the flight program is to isolate the benefits of specific technologies. However, when one considers the complex interactions occurring in the flight environment and the difficulty of extracting specific parametric variations from the available data, the task takes on herculean proportions.

A cooperative program has been defined between the Fluid and Flight Mechanics Branch at NASA Ames/Dryden and the High-Reynolds-Number Aerodynamics Branch at NASA Langley to support and complement specific flight test objectives. In addition to the flight test elements, the program consists of wind tunnel experiments and computational fluid dynamics to enhance the understanding of interacting technologies and to isolate individual benefits. The following sections will present brief overviews of the flight and ground experimental elements and a more complete discussion of the computational support.

This paper will mainly address issues and questions associated with the forward swept wing and closely coupled canard. The primary focus will be on research questions which must be addressed to obtain high quality ground and flight test data. These data will be used in conjunction with computational predictions to complement the analyses required to comprehensively understand the interacting technologies.

BENEFITS OF THE X-29A WING AND CANARD

Before the three phases of the program are discussed, it is appropriate to include a brief discussion of the benefits associated with the forward-swept wing and the canard. For transonic flight, wing sweep is used to delay the onset of drag rise. Uhad, et al. (ref. 1) demonstrated experimentally that a forward-swept wing offers potentially lower wing profile drag than an equivalent aft-swept wing for a transonic maneuvering design point. This yields higher sustained lift coefficients at transonic maneuvering conditions. If one compares aft- and forward-swept tapered wings, the local sweep angles for the forward-swept wing increase as one progresses from the wing leading edge to the trailing edge, while the opposite is true for an aft-swept wing. This results in lower wave drag losses for similar flow conditions and shock locations. Moore and Frei (ref. 2) similarly showed that the trade-off between forward- and aft-swept wings could favor the forward-swept wing. Their comparison configurations

held the wing area, aspect ratio, taper ratio, and shock sweep constant between the forward- and aft-swept wings. The forward swept wing had significant reductions in the wing bending moment at the pivot resulting from an inboard shift in the wing center of pressure. If one maintains the same shock sweep for the comparisons, the forward swept wing has a lower leading-edge sweep. This allows specific supercritical airfoils to be used which have demonstrated reductions in profile drag with decreasing leading-edge sweep. If one imposes a constraint of constant bending moment at the pivot and removes the constraint of constant aspect ratio, the forward-swept wing yields a higher aspect ratio in comparison to the aft-swept wing. This, of course, is beneficial in reducing induced drag.

Improved handling characteristics for forward swept wings at higher angles of attack were demonstrated in an experimental wind tunnel program (ref. 3). In general, flow separation on a forward-swept wing begins inboard and progresses toward the wing tip. In contrast, the tendency for an aft-swept wing is for the wing tip to separate first with the separation progressing inboard. The X-29A wing shows a mild break in the lift curve slope at low speeds and moderate angles of attack (10-12 degrees) resulting from inboard separation. However, the lift and pitching moment data are well behaved to high angles of attack with no pitch-up tendencies. Data also showed the X-29 full-span ailerons can maintain adequate roll control to very high angles of attack.

In addition to the benefits derived form the forward-swept wing, the close-coupled canard yields distinct advantages for the configuration. The canard and wing were designed in conjunction to yield an approximately elliptical span loading distribution on the wing at the maneuver design point. The canard is in the strong upwash field of the wing which results in an effective moment arm at subsonic speeds which is twice that of the geometric moment arm. Another advantage of the close-coupled canard results from the effect of the canard downwash on wing-root separation. At higher angles of attack, the lift generated by the canard to trim the configuration results in a downwash over the inboard part of the wing. This allows the inboard flow to stay attached to higher angles of attack than would be possible without the canard influence. The effect of the canard on the wing loading is presented in figure 2. These data are from the 1/8-scale model test at NASA Ames (ref. 4). The strong influence of the canard on wing span loading is evident as the canard deflection angle is changed at a given angle of attack. The loading is markedly shifted outboard as the canard deflection is increased.

FLIGHT TEST PROGRAM

As a subset of the flight-test objectives for the complete X-29A flight program, specific objectives have been identified which are associated with the forward-swept wing and close-coupled canard. To meet these objectives, extensive data must be gathered and analyzed over a wide range of flight conditions. The aircraft has been extensively instrumented to gather these data, and software has been developed to assist in data manipulation and analysis. Figure 3 indicates some of the instrumentation which will be used. Static pressure orifices are arrange in five rows on the wing (η = 0.2, 0.31, 0.49, 0.70, and 0.91) and two rows on the canard (η = 0.28 and 0.65). These pressure data are extremely informative relative to inferences concerning wing-canard interactions and stall onset and progression. In addition, in-flight flow visualization will also be used to qualitatively identify flow characteristics through the use of flow cones. These are similar to tufts having a small plastic cone attached to the free end to enhance visibility and increase durability.

One of the potential problems associated with a forward-swept wing is aeroelastic divergence. In order to build a wing using conventional materials and manufacturing techniques strong enough to counteract this divergence, a significant weight penalty is incurred. Krone (ref. 5) presented the concept of advanced aeroelastically tailored composites, which are used in the X-29A vehicle, to overcome this problem. The concept uses a buildup of specifically oriented plies of composite laminate to form the wing skins. The orientation and characteristics of the plies can be designed to have the strength necessary to overcome divergence. An additional advantage is that the technique can be used to tailor the aeroelastic twist distribution at maneuvering conditions.

A wing-deflection measurement system is installed on the right wing of the flight-test aircraft. Two fuselage-mounted receivers with different focal lengths are used to monitor 12 targets mounted on the

wing surface, figure 3. These data can be reduced to determine discrete deflections at each of the targets or integrated to determine the average twist angle and section translation for the various span locations. These data will have several uses including validation of structural design methodology. The data are critical in order to provide valid, reliable, transonic computational predictions of the configuration flow field for the flight vehicle. The supercritical wing is an efficient but sensitive performer at transonic speeds. Small changes in flow conditions or geometry (such as aeroelastic deflections) can have significant effects on the flow over the wing surface including shock location, shock strength, flow separation, and buffet onset.

A number of challenges have been encountered as the flight-test program has progressed. Some of these difficulties have centered around data analysis. The aircraft's negative static margin and the use of canard, wing flaps, and strake flap simultaneously, figure 1, for pitch control make it exceedingly difficult to separate the effect of specific variables. In normal flight the deflections of these control surfaces are controlled by the Automatic Camber Control (ACC) system. Hence, the ability to isolate specific stability derivatives is quite limited. However, the Manual Camber Control (MCC) system was implemented to limit the number of parameters allowed to vary for control purposes. This allows the flap to be fixed at a discrete setting during a given portion of the flight, thereby reducing the number of control surfaces whose deflections are varying. An example of different inferences derived from data for similar flight maneuvers using the two different modes (ACC and MCC) is presented by Waggoner, Jennett, and Bates in reference 6.

NTF MODEL AND WIND TUNNEL TEST

A 1/16-scale model of the X-29A, figure 4, is being designed and fabricated for testing in the National Transonic Facility (NTF) at NASA Langley. The NTF was conceived to provide high-Reynolds-number test capability for aerodynamic research and development testing of commercial and military aircraft configurations. The NTF is a closed-circuit, single-return, fan-driven, wind tunnel capable of continuous operation over a Mach number range of 0.2 to 1.2. It is capable of operating at very low temperatures (−320°F) by injecting nitrogen at cryogenic temperatures into the stream. By operating at elevated pressures and cryogenic temperatures, a maximum chord Reynolds number of 120 million at Mach number of 1.0 for a chord of 0.82 feet is achievable (ref. 7).

The X-29A test program is intended to provide significant data which will complement the flight-test program. In addition to providing basic data for flight-to-tunnel and code-to-tunnel correlation studies, Reynolds number effects on a number of sensitive flow areas will be investigated. Over the complete NTF testing schedule for the X-29A, it is anticipated that Reynolds number effects will be determined on wing surface pressures and wing-canard interactions; supercritical design; shock/boundary layer interactions; performance, stability and control; and high-angle-of-attack characteristics.

1/16 SCALE MODEL

The NTF model has been fabricated by Grumman Aerospace Corporation under contract with NASA Langley. The model can be used to simulate aerodynamic control surface deflections through the use of variable incidence canards and interchangeable sets of wing flaperon, rudder and strake flap parts. The design of the model allows for the simulation of four wing flap settings, seven strake flap settings and four rudder settings. In addition, six positions are available for the variable incidence canard. The external lines of the X-29A are modeled in significant detail. Flow through nacelles will afford the first simulated inlets for cryogenic operation in the NTF. The flow through ducts will simulate the mass flow rate for a condition near the cruise design point. Although the provisions to simulate various mass flow rates are not anticipated, the calibration of the inlets for various Reynolds numbers presents a significant challenge.

Data acquisition planned for the test program includes aerodynamic force and moment data, wing pressure distributions and wing deformation characteristics. An extensive array of instrumentation will

support this task. Static pressure orifices are located at span locations corresponding to wing stations 50 and 114. The orifice locations were chosen to correspond closely to the orifice locations on the number-one flight-test aircraft. A 48-port electronic sensing pressure (ESP) module will be mounted in the model nose, as well as an accelerometer-type angle of attack indicator.

Two, six-component, 1.75-inch diameter, internal strain-gage balances have been constructed. Each is intended to be used over a different load range. The normal force design loads of the two balances are 1500 and 2500 pounds. It was desirable to have static pressure measurements on the canards. However, because of the size of the canard (1/8-inch thick at mid-span) and small diameter of the shank attachment to the fuselage, it was not feasible. In lieu of this, a three-component strain-gage balance is built into the left canard to measure shear, bending and torsion. A wing-root bending-moment gage allows for real-time evaluation of model dynamics.

Deflection of the wings during the wind tunnel test will be measured by use of a video model deformation system. These measurements will be used to determine the magnitude of differences in wing shape between the model and flight vehicle under similar flow conditions.

The fabrication of the model was somewhat unique. The left wing and fuselage half and right wing and fuselage half were each machined as one piece out of a high-nickel-content steel suitable for cryogenic models (Vascomax 200). The two halves were then welded together yielding a one-piece wing fuselage model. The interchangeable flaps also presented a serious design problem. The flap elements are quite thin and were designed to attach to the wing through a tongue-in-groove arrangement. This design was necessary to ensure compatibility with the severe thermal test environment. The thin tongues on the flaps and the precision machine work for the grooves presented a challenge for the model craftsmen.

NTF MODEL TEST PROGRAM

The model design point simulates flight Reynolds number at M = 0.9 and 30,000 ft. with the NTF operating at minimum tunnel dynamic pressure. Simulated 8-g flight at these conditions yields a $C_N \cdot q$ limit of 2,700 psf for the 1/16-scale model. A comparison of the tunnel-test-to-flight envelope is presented in figure 5. Superimposed on the envelope are the sting divergence limit boundary for the low-angle of attack support system and the envelope of Reynolds numbers attainable with this model in the NASA-Ames 11-Foot Tunnel. Because of the versatility of the NTF, note that even with the sting divergence limit imposed, much of the airplane flight envelope below M = 1.2 can be simulated with the 1/16-scale model in the NTF. At Mach numbers less than 0.7, the entire angle-of-attack range can be tested at flight Reynolds numbers for the entire flight envelope.

The model will be tested over a Mach number range from 0.3 to 1.2 at Reynolds numbers from 2 to 35 million. Initially, the angle of attack will be limited to 20° ; however, with the high-alpha sting, angles of attack up to 60° can be achieved.

COMPUTATIONAL SUPPORT OF THE X-29A EXPERIMENT

A comprehensive computational program has been identified to support both flight and ground testing of the X-29A. The effort up to the present time has concentrated on the applicability of potential flow methods. The following sections will briefly describe the codes which have been used, describe the code calibration effort and present selected results.

COMPUTATIONAL TECHNIQUES

Three primary computational techniques have been identified to support the initial computational phase of the program. A three-dimensional, small-disturbance, transonic analysis code for wing-fuselage-canard combinations (CANTATA), a three-dimensional full-potential, transonic analysis code for wing-fuselage combinations (TAWFIVE), and an aerodynamic/structural analysis system (TAPS) will be

employed to exploit the advantages of each technique. Salient features of the computational techniques are discussed below.

CANTATA Analysis Code - The Canard/Tail Transonic Analysis code (CANTATA, ref. 8) is characterized by a unique grid-embedding technique which provides excellent resolution for either a wing-fuselage-canard or wing-fuselage-tail configuration. The code solves for the flow field about the configuration of interest in the direct mode employing an ADI scheme. Design via numerical optimization is available in the code but is not anticipated to be used in the current application. Using finite difference approximations, a modified small-disturbance potential-flow equation is iteratively solved in a system of multiple embedded grids. The modifications to the classical small-disturbance equation are in the form of extra terms, which, when added to the equation, provide more accurate resolution of shock waves with large sweep angles and a better approximation of the critical velocity where the full-potential equation changes from elliptic to hyperbolic type.

Viscous effects are approximated by coupling a modified Bradshaw boundary-layer computation to the finite-difference potential-flow solution. The modified method provides a technique to extend a two-dimensional boundary-layer calculation to account for first order viscous effects (ref. 9). The viscous effects are incorporated in the solution by adding the boundary-layer displacement slopes to the wing surface slopes. This modifies the wing surface to an equivalent "fluid" wing shape which is then analyzed by the potential flow code.

The basic concepts inherent to the code have been extensively validated by several researchers (refs. 10-12). These studies have, in general, been for aft-swept wings and for single lifting surface configurations.

TAWFIVE Analysis Code - A computer code for the Transonic Analysis of a Wing and Fuselage with Interacted Viscous Effects, references 13 and 14, is also used in this study. The code utilizes the interaction of three-dimensional inviscid and viscous flow solvers to obtain transonic flow-field solutions about wing-fuselage combinations. The outer inviscid flow field is solved using a conservative, finite volume, full potential method based on FLO-30 by Caughey and Jameson (ref. 15). No modifications were made to the internal grid-generation algorithm in FLO-30, which is a body-fitted, sheared, parabolic coordinate system.

A three-dimensional boundary layer for the wing is computed using a compressible integral method. The code has the capability of computing laminar or turbulent boundary layer with the methods of Stock (ref. 16) or Smith (ref. 17), respectively. An important feature of the code is Street's treatment of the wake (ref. 13). The wake model used in FLO-30 was replaced with a model which satisfies flow tangency on the wake displacement body and the pressure jump condition resulting from wake curvature. These changes in the code can make significant differences in results obtained on various configurations.

Transonic Aeroelastic Programs System - The Transonic Aeroelastic Program System (TAPS) developed by Campbell (ref. 18) is a method which allows the effects of static aeroelastic wing deflections to be included in steady transonic aerodynamic calculations. The method interacts a three-dimensional transonic computer code with viscous effects and a linear finite element structural analysis code to calculate wing pressures and deflections. The nonlinear nature of the transonic flow makes it necessary to couple the aerodynamic and structures codes in an iterative manner. TAPS has been arranged in a modular fashion so that different aerodynamic or structural programs may be used with a minimum of coding changes required.

For the current study the TAPS program has been utilized to help understand the correlations of computations and wind tunnel data with data obtained from the flight test. The flight vehicle has been analyzed in the TAPS program to predict the wing deflections under flight loads. These calculations will be described in detail in a subsequent section.

CODE CALIBRATION EFFORT

The first phase of the computational effort will involve calibration of the transonic aerodynamic codes for application to the X-29A configuration. Although these codes have been applied to numerous configurations, the X-29A is such a unique configuration that a calibration phase is required. This utilizes

both code-to-code and code-to-experiment comparisons. In general, for transonic analysis codes in widespread use for analysis and design, there exists an inverse relationship between the physics included in the governing flow equations and the complexity of geometry for which one is realistically capable of obtaining a solution. The two transonic potential flow codes discussed previously illustrate this point. The TAWFIVE code solves the full-potential flow equation coupled with a three-dimensional boundary-layer analysis for a wing-body configuration. The CANTATA code, on the other hand, solves a simplified flow equation (extended small disturbance) on a more complex (wing-fuselage-canard) geometry.

The X-29A has a very complex geometry from a computational standpoint. The body, figure 6, was extremely difficult to model, particularly in the wing-fuselage juncture region. The discontinuous trailing edge resulting from the body strake geometry offered another challenge. The effects of the inlet on the flow over the canard and the dihedral effects for the wings were unknown. In addition, there is little experience to draw from in solving flow fields including viscous effects about swept-forward wing configurations. Hence, there were a number of compelling reasons to undertake the code calibration phase of this effort.

The first task addressed was to generate a detailed computational model of the fuselage, figure 6. The objective was to make as few compromises as possible to the geometry while generating a model for which computational mappings could be generated by the codes. The wing and canard geometry has also been modeled; however, this has been a much more straightforward task. The compromises to the wing geometry consisted of a modified trailing edge in the vicinity of the body stake for each of the codes and modeling a wing without any dihedral in the CANTATA code because of its Cartesian grid structure.

The actual comparisons on the configuration have been performed in a systematic manner. The approach will be described here and selected comparisons from the various steps will be presented in the following section. The initial computations were performed on the wing-fuselage combination using the TAWFIVE and CANTATA codes. These computations were also compared to available wind tunnel data on the wing-fuselage configuration. The differences between the computations and experimental data were evaluated in light of previous experience. Code-to-code differences were analyzed in light of known differences (full-potential vs. small-disturbance, conservative vs. non-conservative, etc.) between the codes on computational results. Comparisons have also been made between computations on the fuselage-canard geometry. Each of these sets of calculations and comparisons will help to understand the wing-canard interactions. These analyses will also allow the wing-fuselage-canard configuration to be analyzed with significantly greater confidence than if the full configuration were analyzed initially.

Computations on the wing-fuselage-canard configuration in the CANTATA code have been compared between available wind tunnel data on the 1/8-scale model and flight data. The available experimental data was surveyed to determine if comparable test points existed between the wind tunnel and flight tests. Comparisons of these data were accomplished at appropriate conditions. Differences between these data were attributed to either aeroelasticity or Reynolds number. Calculations with the TAPS program were accomplished to investigate aeroelastic effects. These data were compared with deflection measurements from the flight system.

The use of any computational technique benefits from the accuracy inherent in the method. However, it is also realized that a code can be used effectively if one understands the computational limitations and the effects of any inaccuracies which may be present. This becomes increasingly important as one approaches the boundaries of practical applicability for a given code. The approach undertaken in this study has identified some practical limitations of the computations for this complex configuration.

SELECTED COMPARISONS

Initially, computations were performed on the X-29A wing-fuselage combination and compared with available wind tunnel data from the 1/8-scale model tested at NASA-Ames (ref. 4). Results are presented for a subsonic Mach number (M = 0.6) and a high-transonic Mach number (M = 0.9). The computational results are inviscid with no aeroelastic effects included. The transonic analyses were performed at the experimental angles of attack and Mach numbers. These results demonstrate the code-

to-code differences and cover the range of applicability for the codes up to flow conditions where the flow shows sign of significant separation on the wing.

Results are compared at M = 0.6, α = 7.7°, in figure 7. The comparisons are quite good at this condition. Notice that generally the full-potential code (TAWFIVE) predicts more expansion at the leading edge on the upper surface. Because of the grid density at the trailing edge, the CANTATA results seem to be more sensitive to the flaperon geometry. Also note the differences in the computational predictions at the wingtip. The TAWFIVE code predicts the upper-surface leading-edge peak quite well. However, the small-disturbance results compare better with the experiment aft of the leading edge.

The comparison presented in figure 8 are at M = 0.9 and α = 6.9°. The comparisons on the outboard part of the wing are fairly good, although the experimental results show trailing-edge (η = 0.7) and shock-induced (η = 0.49) separations. On the inboard portion of the wing, the lower surface pressures are predicted fairly well; however, the upper surface pressures show some discrepancies. At η = 0.31 and 0.19 the experimental and computational results on the upper surface forward of the shock do not match well. While the experimental data are sparse in this region, it does not appear that the characteristics of the flow are predicted with either computational technique. In general, the two codes predict similar flow patterns over the wing span for the flow conditions observed. Comparisons for the fuselage-canard configuration also showed consistent predictions between the two codes.

The next step in the calibration effort involved computations on the wing-fuselage-canard configuration. The first significant incongruence between the actual configuration and the geometric capabilities of the CANTATA code was uncovered. The grid structure for both the canard and wing grids is Cartesian. This results in the boundary conditions for both surfaces being applied in parallel planes. Because of the dihedral in the wing, the locus of wing leading-edge points intersects the canard wake. This in conjunction with the closely coupled lifting surfaces results in a significant interaction between the wing and canard. The comparison presented in figure 9 shows the effect of relative wing-canard vertical position on the wing pressure distribution near mid span. The calculations were made with the wing 3 inches (full scale) above and below the plane of the canard. When the wing is positioned above the canard plane, the loading over the inboard wing sections is collapsed. By comparisons with wind tunnel experimental data, it became obvious that positioning the wing slightly below the canard yielded the most reasonable flow simulation.

Comparisons between wind tunnel data from reference 4 and computational predictions for the complete configuration are included in figures 10 and 11. The comparisons are strikingly similar for these M = 0.9, low lift (figure 10) and M = 0.95, moderate lift (figure 11) conditions. The inboard region on the uppers surface is predicted adequately. As one observes the comparisons outboard of the leading-edge break, the characteristic of the experimental pressures on the upper surface is not captured in the computations. This difference was observed in all the comparisons at M = 0.9 and above. The pressure distribution on the canard is predicted reasonably well except at the leading edge on the upper surface. An expansion observed in the experimental data is not evident at all in the computations. This difference could be the result of geometric compromises related to the inlet or to a vortex originating from the forebody or inlet lip. The accentuated expansions and compressions near the wing trailing edge are the result of computationally modeling the discrete hinge-lines for the segmented trailing-edge flap system. Based on these comparisons at the higher Mach numbers, plus comparisons at subsonic conditions, it was felt that an adequate computational model had been generated.

At this point the focus on the experimental data shifted from the data obtained in the controlled wind tunnel environment to data obtained in the dynamic flight environment where the uncertainties are increased. Before proceeding with comparisons between the computations and the flight test data, it was of interest to determine how well the flight and wind tunnel data compared. Because of the large number of parameters which had to be matched (Mach, angle of attack, canard, wing flap, and strake flap deflections, etc.), only a few conditions were identified for comparison between the wind tunnel test and flight test. Comparisons at M = 0.8 and M = 0.9 are presented in figure 12. At M = 0.8 and α = 2.2°, the comparisons between flight and wind tunnel data are excellent at both of the span stations shown. At higher Mach numbers and angles of attack the comparisons were not quite as good. It was interesting to note, as shown in figure 12b, that a very good comparison was obtained when the tunnel data were compared at an elevated angle of attack relative to the flight data. Several hypotheses

were purposed to explain this anomaly including wind tunnel wall interference, Reynolds number effects, and aeroelastic deformation. Wing deflection data were available at some flight conditions. A flight test point of interest was identified and the configuration was analyzed in TAPS. The resulting predicted deflections are compared with the measured deflections in figure 13. The measured deflections from the flight test also show an error range with the data. TAPS overpredicted the deflections along the entire span. However, the inclusion of the computational (overpredicted) deflections in the solution did not yield differences between the rigid and aeroelastic solutions as large as those observed between the flight and tunnel experiments at comparable angles of attack. These anomalies accentuate the need for the experiment in the NTF.

The final set of comparisons is between computational predictions and flight test data at M = 0.6, 0.8, and 0.91 and moderate lift levels (figures 14, 15, and 16). The comparisons at M = 0.6 and 0.8 are quite good on both the wing and canard. At the outboard span location on the wing the upper-surface leading-expansion is slightly underpredicted at M = 0.6. At the inboard location on the wing at M = 0.8 the leading edge expansion is overpredicted in the computations. The upper-surface leading-edge flow is predicted adequately at M = 0.91 for the inboard station yet the level of expansion from 20% to 30% chord is not predicted accurately. At M = 0.91 the characteristic of the upper-surface flow is not predicted at the outboard span location. The characteristics of the experimental and computational pressure distributions are similar to those observed in the comparisons of wind tunnel and computational predictions in figures 10 and 11. The influence of the rather bulbous flap-track fairings is evident in comparisons on the lower surface at the outboard span location for M = 0.8 and 0.91. There was no attempt to model these fairings computationally.

There is evidence of flow expansion at the inboard canard location leading edge for all three Mach numbers which is not predicted computationally. At M = 0.91 the expansion appears to terminate in a shock at approximately 10% chord. While not shown in these figures, this expansion migrates outboard along the canard with increasing angle of attack. Except for this anomaly the canard flow is predicted well.

Overall the comparisons between the experimental data and computational predictions are encouraging. However, there were differences observed for which the causes were difficult to isolate. In particular, at higher Mach numbers the flow on the outboard part of the wing, as well as the canard leading edge was not predicted well computationally. These observations identify the need for obtaining high-Reynolds-number data under controlled conditions.

SUMMARY AND CONCLUSIONS

This paper has presented an overview of a major cooperative effort between NASA Ames/Dryden Flight Research Facility and NASA Langley in support of the X-29A flight-test program. The effort involves flight testing, wind tunnel testing in the NTF, and computational support. Each phase in the effort has distinct advantages and disadvantages relative to the data which are obtained. For example, the flight data could be considered "gospel" without scaling or wall interference effects. However, as was previously discussed, it is difficult to isolate the influences of individual parameters. Wind tunnel testing allows the component build-up and parametric variation of independent variables. Hence, individual influences and interference effects can be isolated. However, the data can suffer from scaling effects and/or wall interference. In addition, although the range of variables tested can cover the airplane capability, testing all combinations of each variable quickly expands to a prohibitively large matrix. While physical geometry and fluid physics modeling comparisons are often made, CFD allows the gaps between tunnel and flight data to be filled. It also allows evaluation of flight conditions outside the cleared flight envelope and estimation of the effects of configuration modifications. Hence, it is easy to see from this simplified discussion that each phase of the effort complements the other phases.

An adequate computational representation of the X-29A configuration has been developed. Comparisons between computational predictions and both flight and wind tunnel experimental data have been made a a range of transonic conditions. At freestream Mach numbers less than 0.9, the comparison of pressure distribution between the computations and experiment is quite good on both the wing

and the canard. Anomalies have been observed for moderate lift coefficients at M = 0.9 and above. The computations show no evidence of the flow expansion observed on the canard leading-edge. In addition, the experimental pressure distribution over the mid-span of the wing has a different character than that predicted computationally. Further computational and experimental investigations of these discrepancies are required to understand these anomalies.

The flight testing of the X-29A aircraft is well under way and a significant amount of data is becoming available. The NTF wind tunnel test model is virtually complete and the NTF test will commence during the Fall 1988. Computational support is continuing with the focus on understanding the anomalies which have been identified. The data available from the three-phase effort will greatly enhance the understanding of the complex flow phenomena and aerodynamics of the X-29A aircraft.

REFERENCES

1. Uhad, G. C.; Weeks, T. M.; and Large, R.: Wind Tunnel Investigations of the Transonic Aerodynamic Characteristics of Forward-Swept Wings. Journal of Aircraft, 20(3), pp. 195-202, March 1983.
2. Moore, M.; and Frei, D.: X-29 Forward Swept Wing Aerodynamic Overview. AIAA Paper 83-1834, 1983.
3. Grafton, S. B.; Gilbert, W. P.; Croom, M. A.; and Murri, D. G.: High-Angle-of-Attack Characteristics of a Forward-Swept Wing Fighter Configuration. AIAA Paper 82-1322, August 1982.
4. Charletta, R.: Series I Transonic/Supersonic Testing in a 12.5% Scale Grumman Design 712, X-29A Forward-Swept Wing Demonstrator Aircraft Model in the NASA ARC 11-Foot and 9x7-Foot Wind Tunnels, at Moffett Field California. AER/T-AMES-538-1-11,97, August 1982.
5. Krone, N. J., Jr.: Divergence Elimination with Advanced Composites. AIAA Paper 75-1009, August 1975.
6. Waggoner, E. G.; Jennett, L. A.; and Bates, B. L.: X-29 Flight Test Program Including Wind Tunnel and Computational Support. SAE Paper 861642, October 1986.
7. Gloss, B. B.: Initial Research Program for the National Transonic Facility. AIAA Paper 84-0585, March 1984.
8. Aidala, P.: Canard/Tail Transonic Analysis. Air Force Wright Aeronautical Laboratories Report AFWAL-TR-85-3087, October 1985.
9. Mason, W. H.; et al.: An Automated Procedure for Computing the Three-Dimensional Transonic Flow Over Wing-Body Combinations, Including Viscous Effects. Air Force Flight Dynamics Laboratory Report AFFDL-TR-122, Vol. I, October 1977.
10. Waggoner, E. G.: Validation of a Transonic Analysis Code for Use in Preliminary Design of Advanced Transport Configurations. ICAS Paper 84-1.4.2, September 1984.
11. Boppe, C. W.: Computational Aerodynamic Design: X-29, the Gulfstream Series and a Tactical Fighter. SAE Paper 851789, October 1985.
12. Rosen, B. S.: Transonic Analysis of Canted Winglets. AIAA Paper 84-0302, January 1984.
13. Street, C. L.: Viscous-Inviscid Interaction for Transonic Wing-Body Configurations Including Wake Effects. AIAA Paper 81-1266, July 1981.
14. Melson, N. D.; and Street, C. L.: TAWFIVE: A User's Guide. NASA TM-84619, September 1983.
15. Caughey, C. A.; and Jameson, A.: Recent Progress in Finite Volume Calculations for Wing-Fuselage Combinations. AIAA Paper 79-1513, July 1979.
16. Stock, H. W.: Integral Method for the Calculation of Three-Dimensional Laminar and Turbulent Boundary Layers. NASA TM-75320, 1978.
17. Smith, P. D.: An Integral Prediction Method for Three-Dimensional Compressible Turbulent Boundary Layers. RAE R&M 3739, 1974.

18. Campbell, R. L.: Calculated Effects of Varying Reynolds Number and Dynamic Pressure on Flexible Wings at Transonic Speeds. NASA CP 2327, Part 1, April 1984, pp. 309-327.

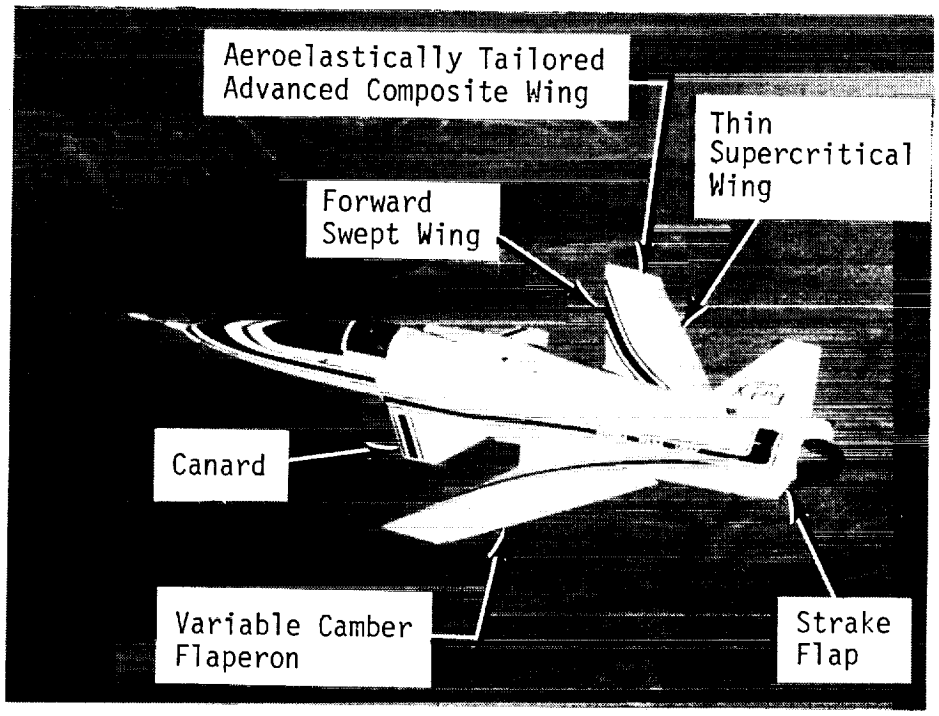

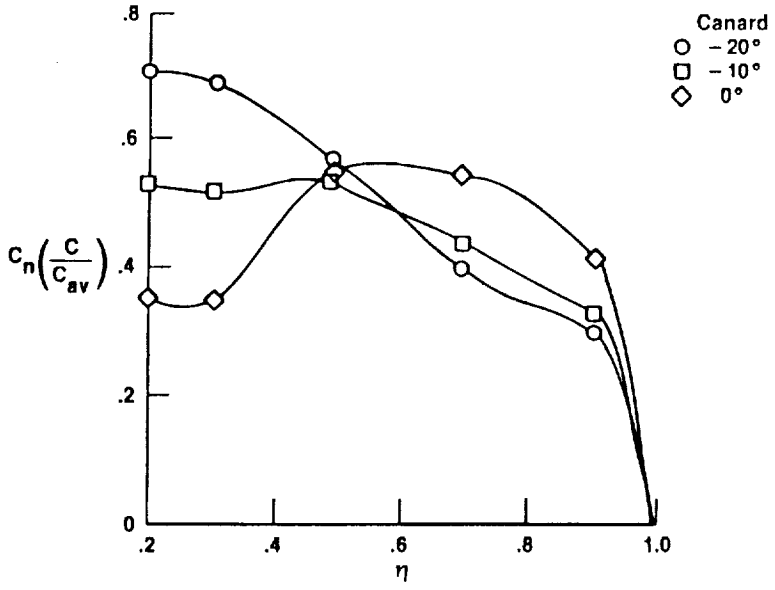

Figure 2 - Comparison of wind tunnel model wing span load for several canard settings

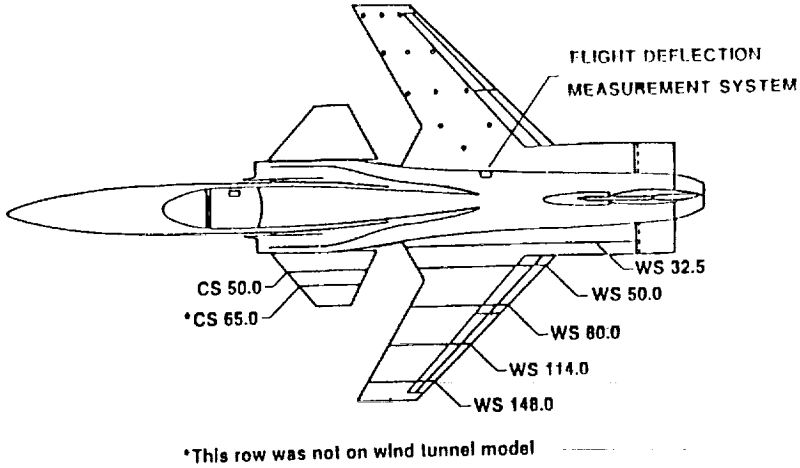

Figure 3 - Static pressure orifice locations and deflection measurement system

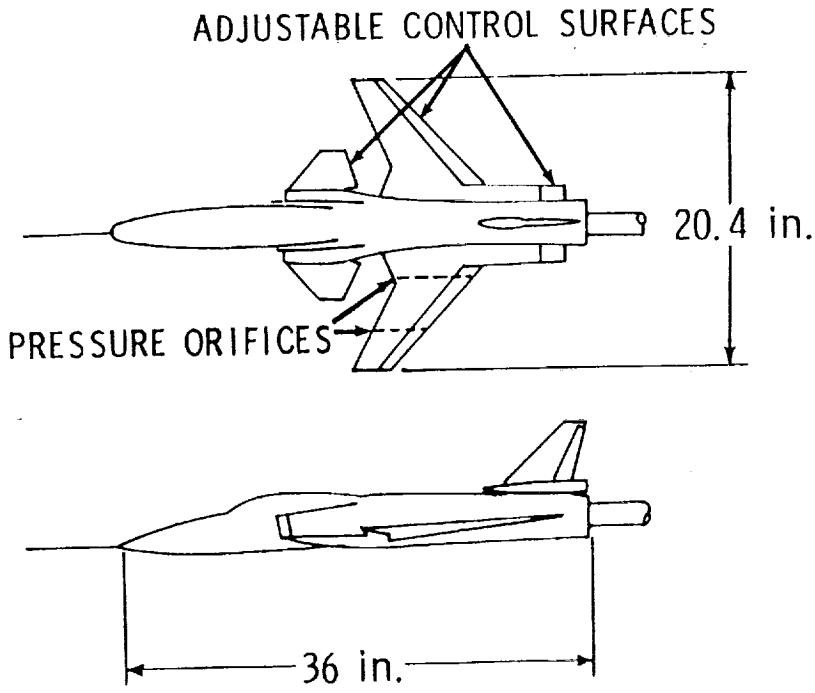

Figure 4 - 1/16-scale X-29 model

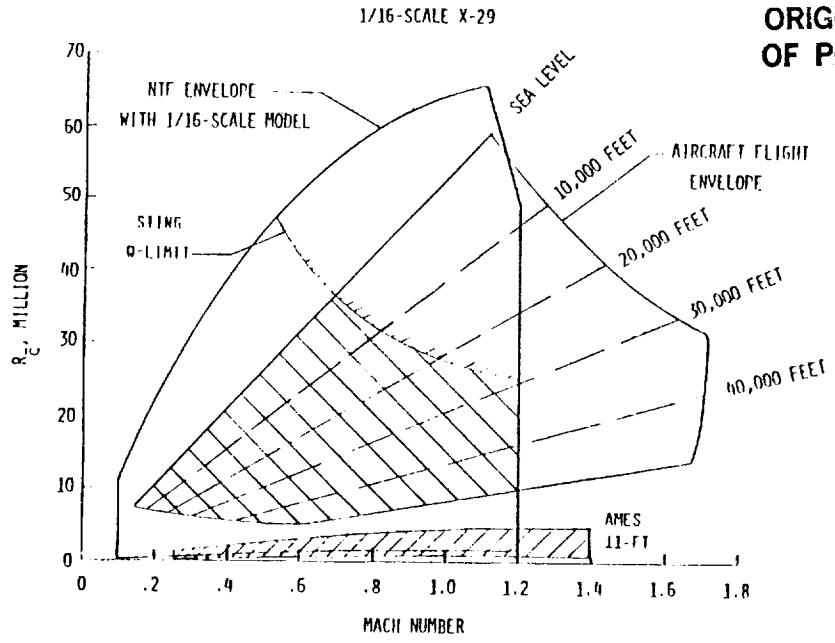

Figure 5 - Comparison of NTF and X-29A flight envelopes

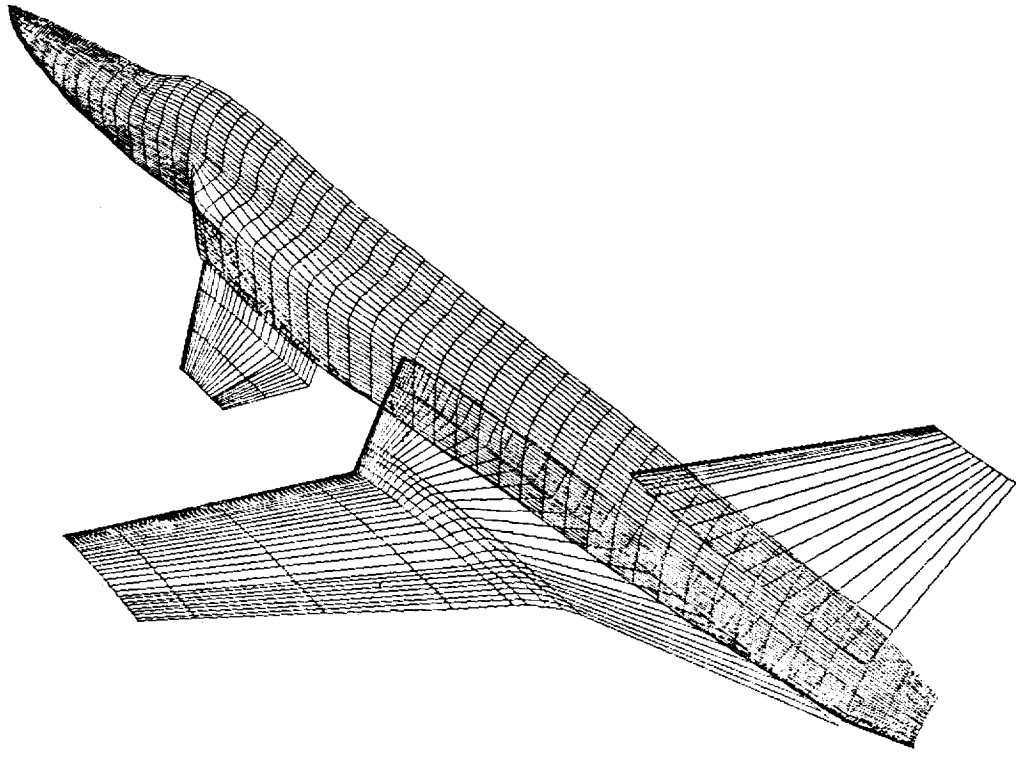

Figure 6 - Wire frame representation of the computational model

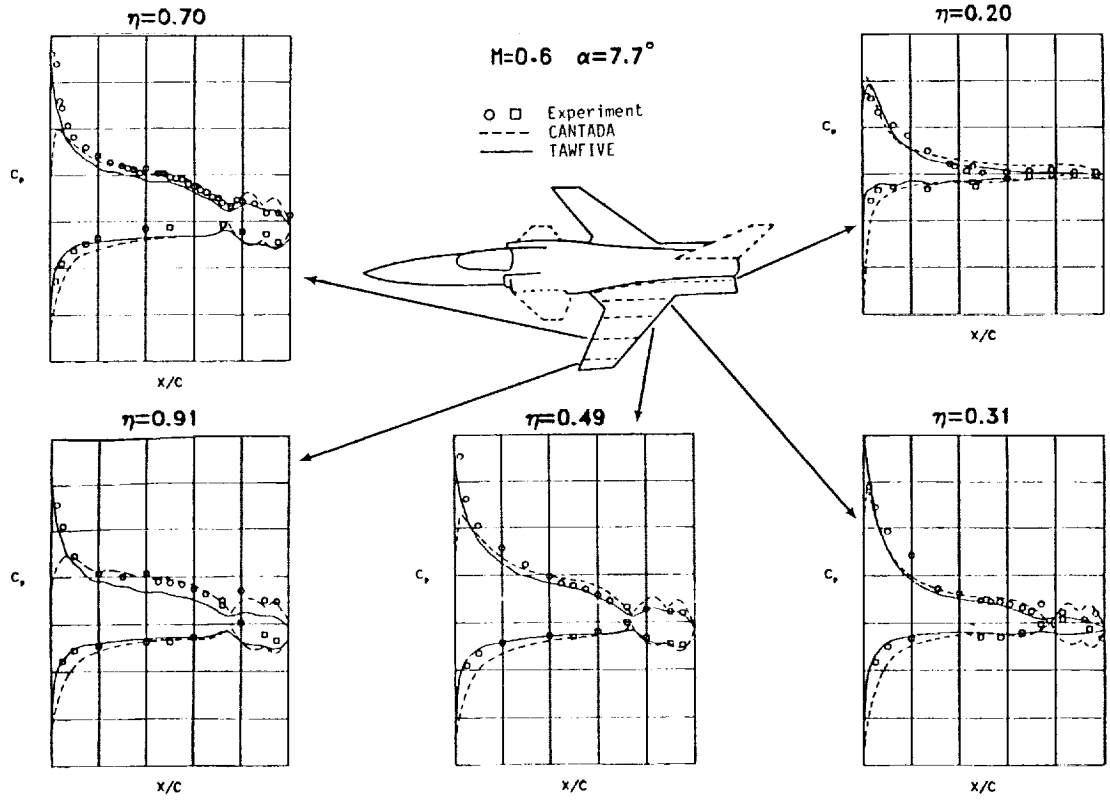

Figure 7 - Comparison of computations and wind tunnel results M=0.6, $\alpha = 7.7°$

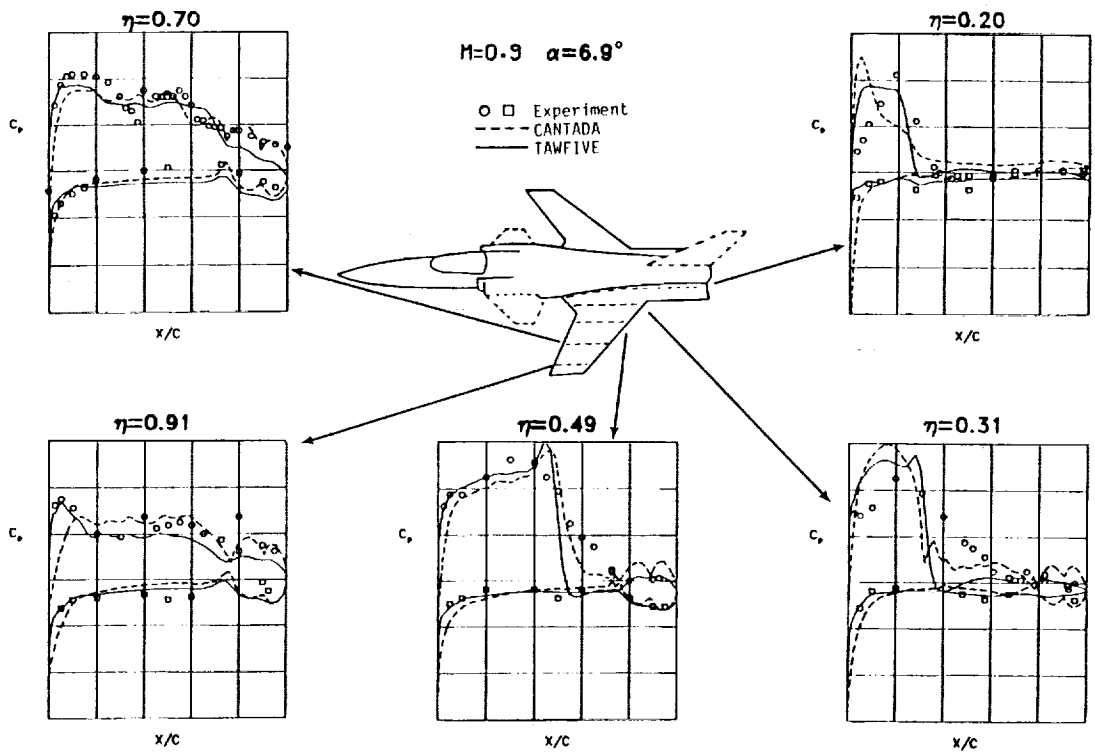

Figure 8 - Comparison of computations and wind tunnel results M=0.9, $\alpha = 6.9°$

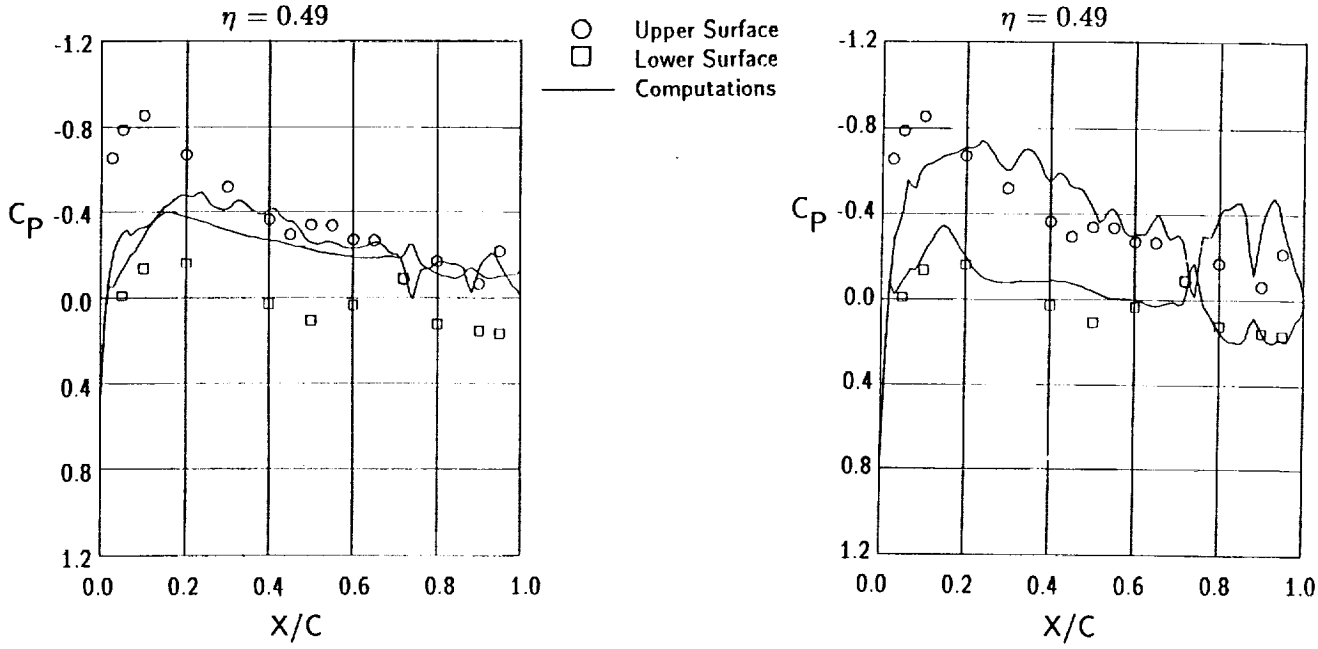

a) Wing above canard

b) Wing below canard

Figure 9 - Effect of wing/canard position on wing pressure distribution - M=0.9, $\alpha = 4.7°$

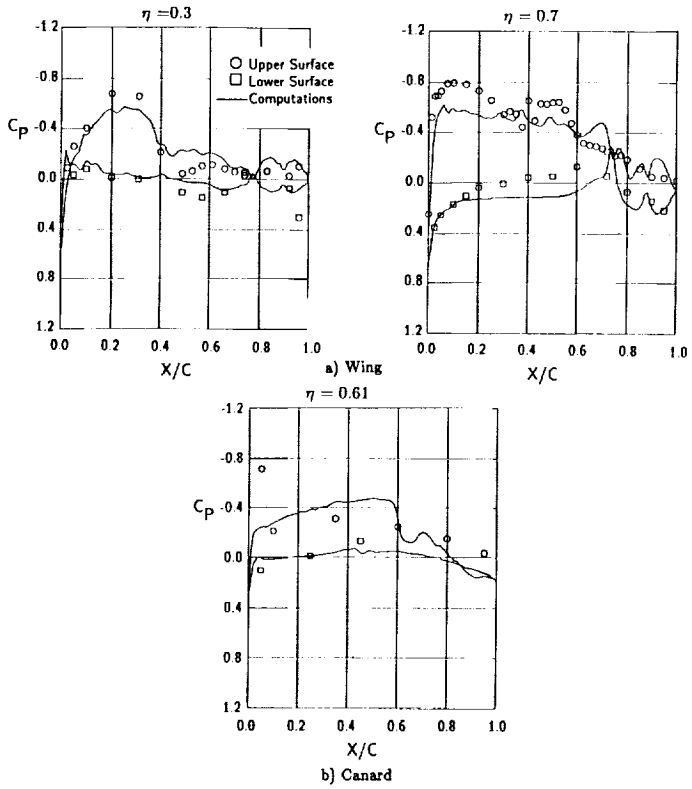

Figure 10 - Comparison of computational results and wind tunnel data - M=0.9, $\alpha = 2.1°$

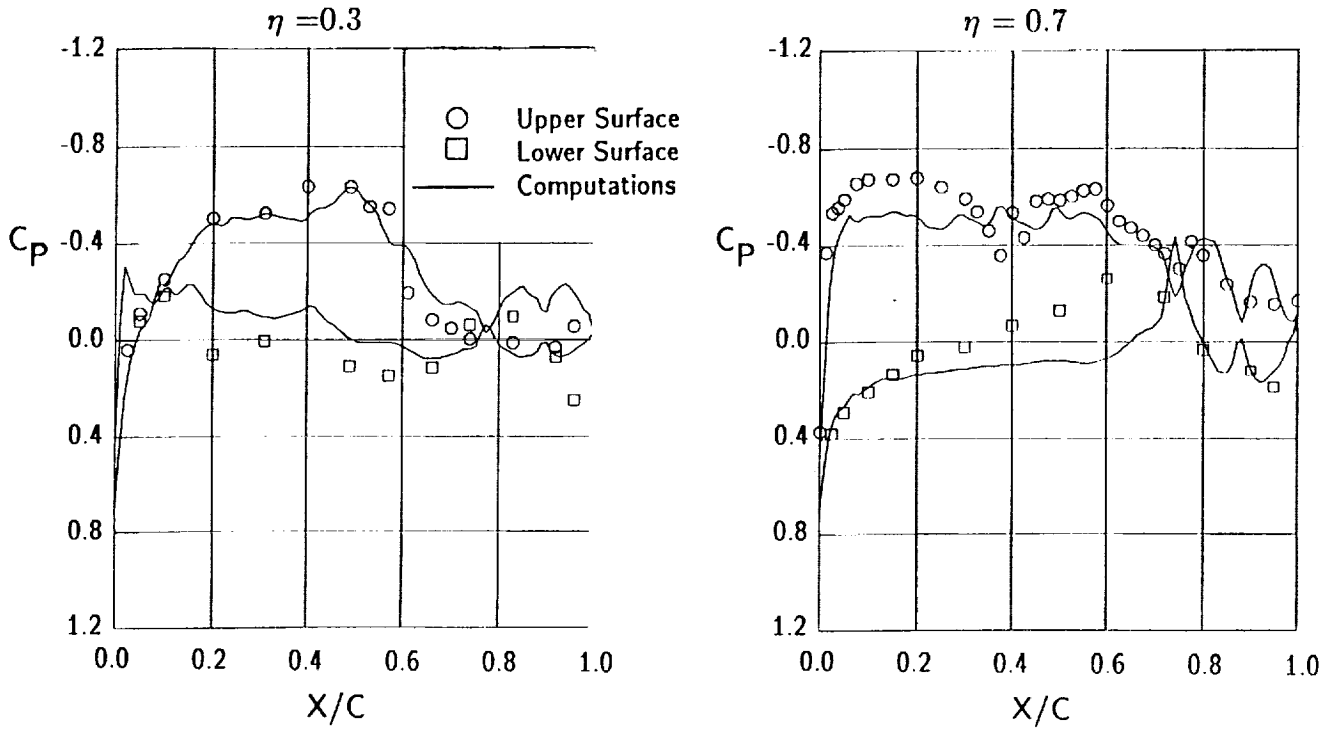

a) Wing

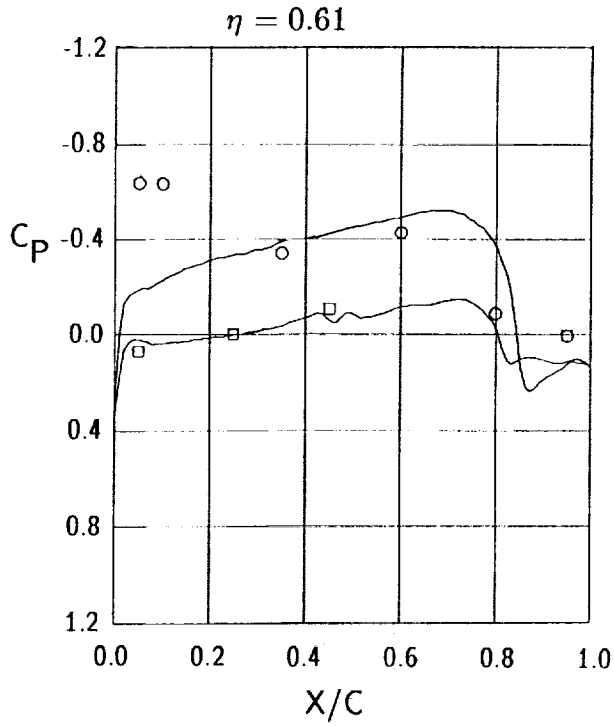

b) Canard

Figure 11 - Comparison of computational results and wind tunnel data - M=0.95, $\alpha = 5.9°$

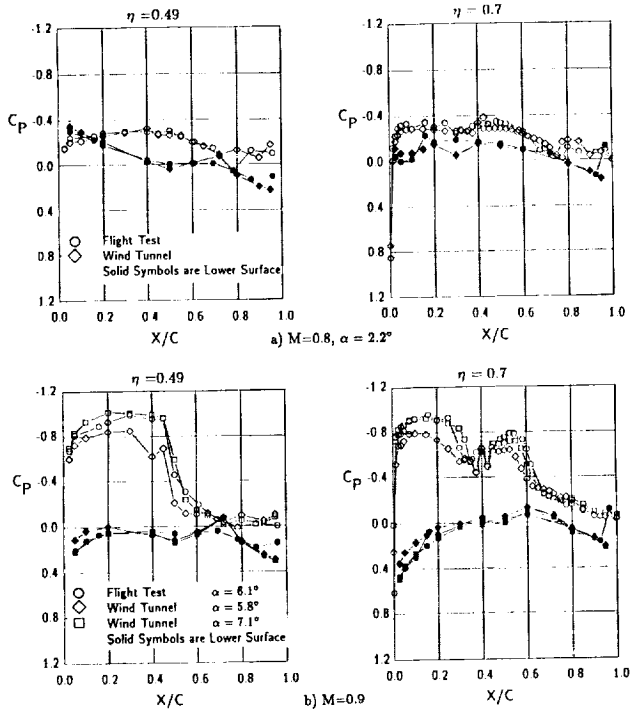

Figure 12 - Comparison of wind tunnel and flight test data

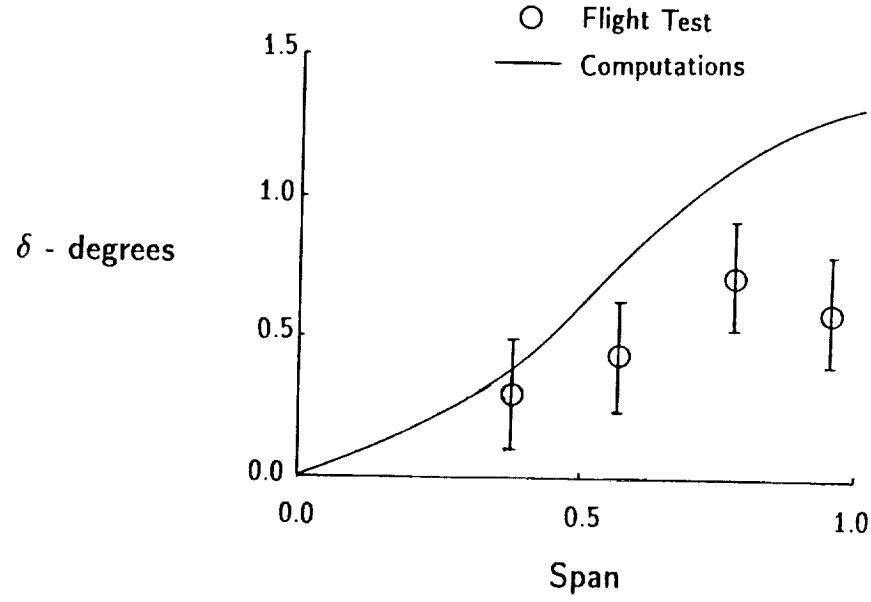

Figure 13 - Comparison of measured and predicted wing deflections - M=0.92, $\alpha = 7.5°$

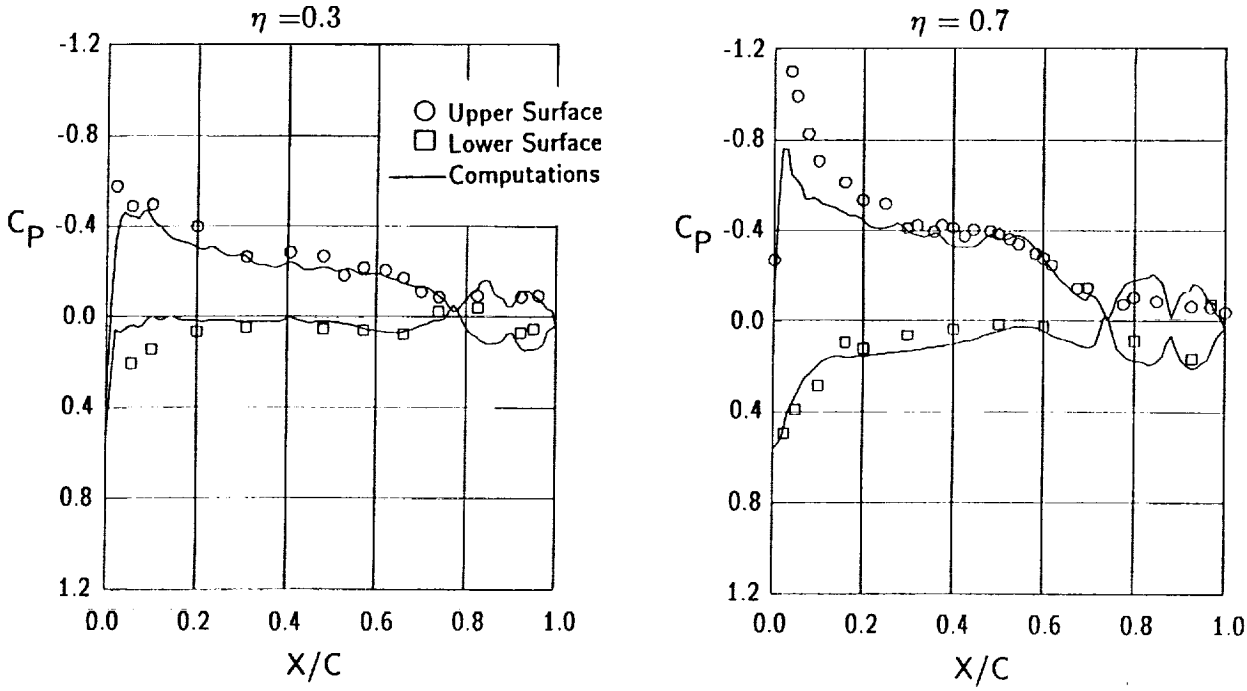

a) Wing

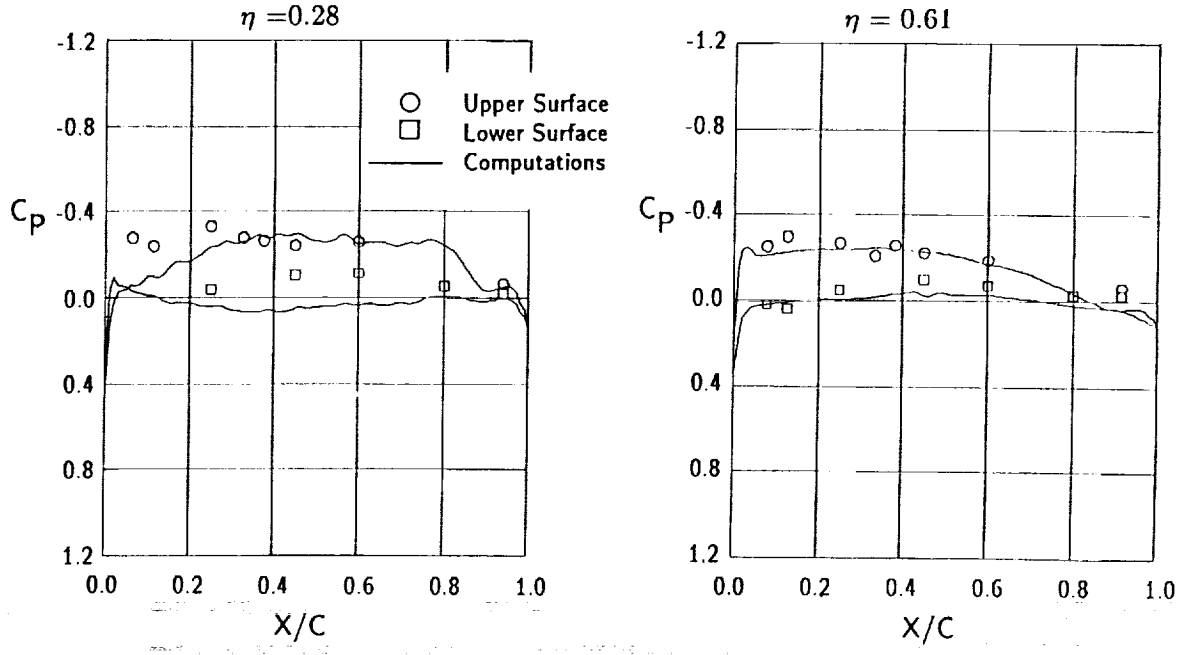

b) Canard

Figure 14 - Comparison of computational results and flight test data - M=0.6, $\alpha = 6.5°$

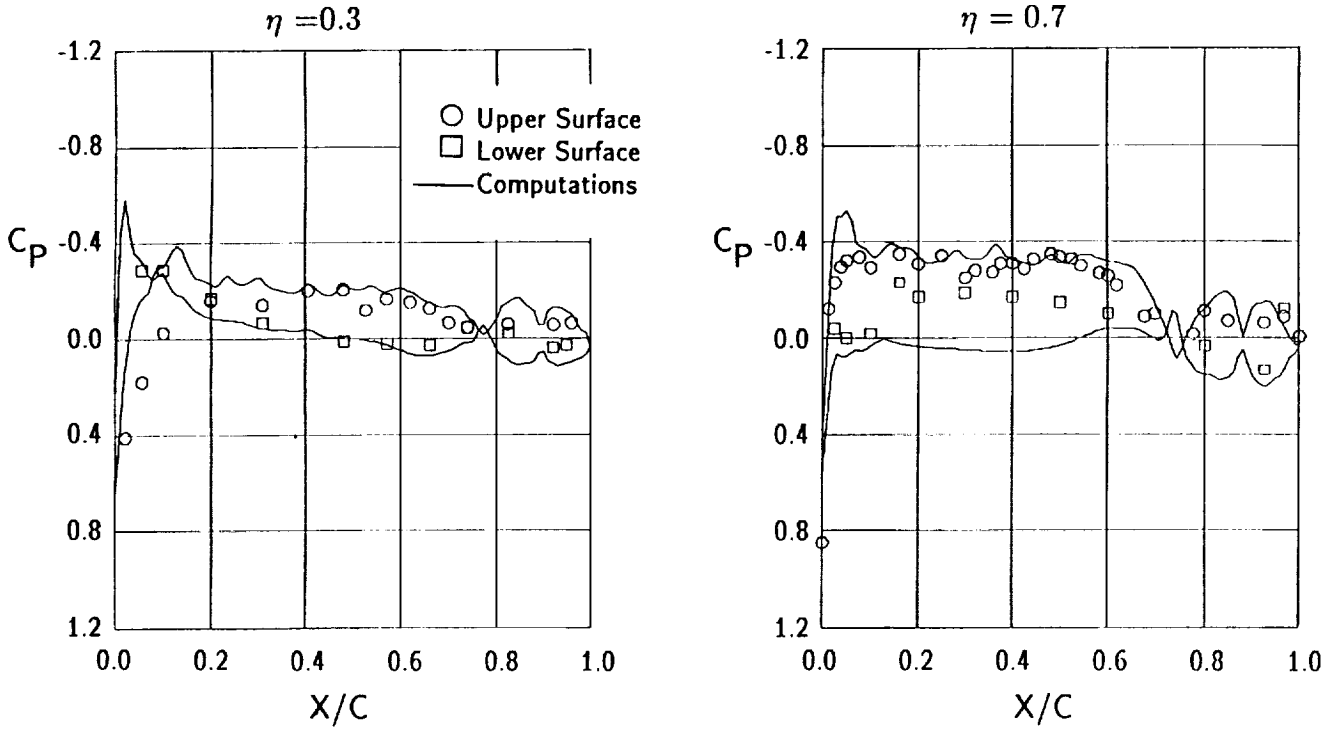

a) Wing

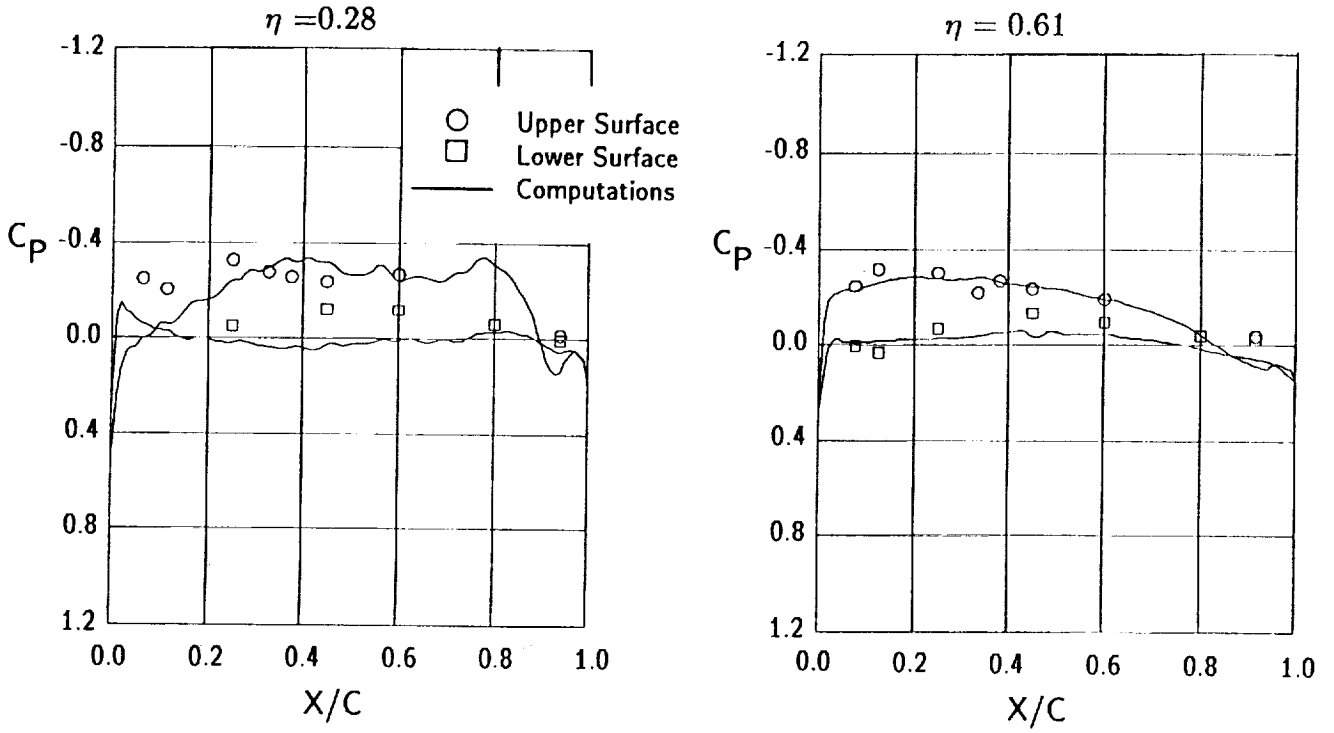

b) Canard

Figure 15 - Comparison of computational results and flight test data - M=0.8, $\alpha = 4.1°$

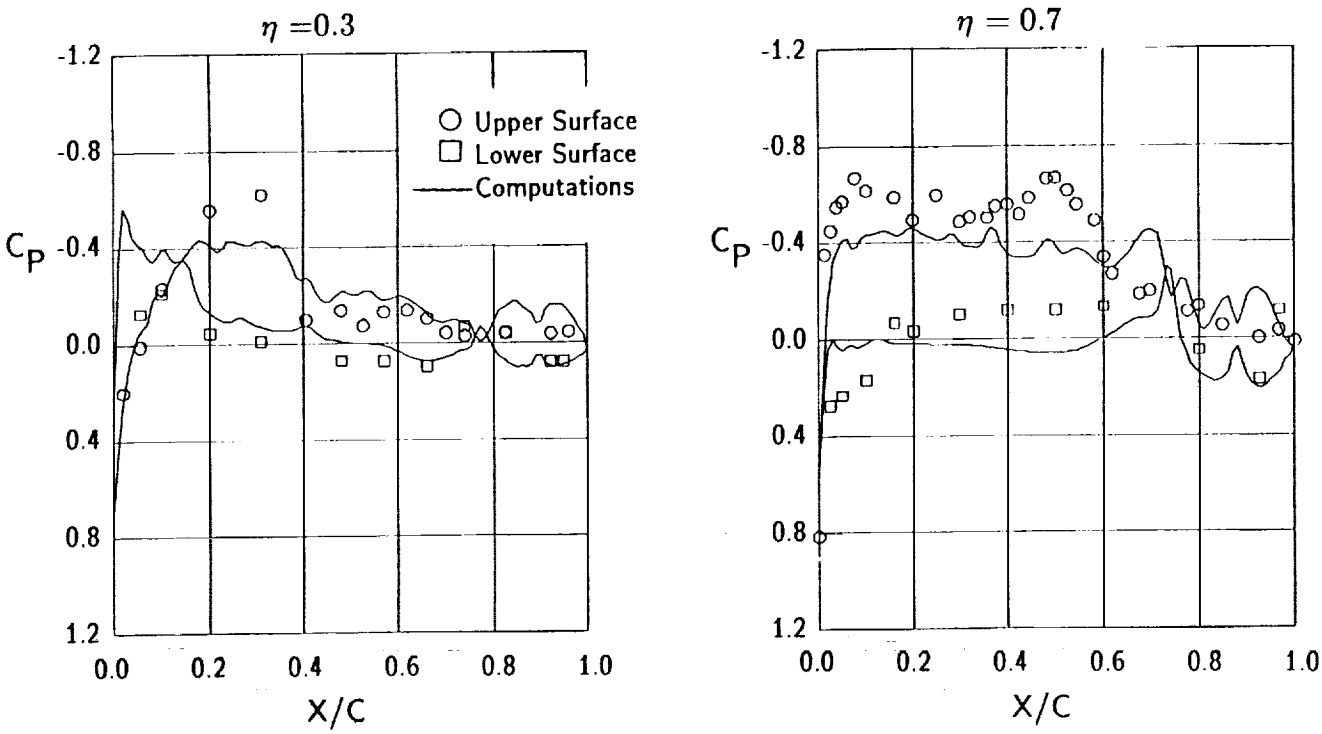

a) Wing

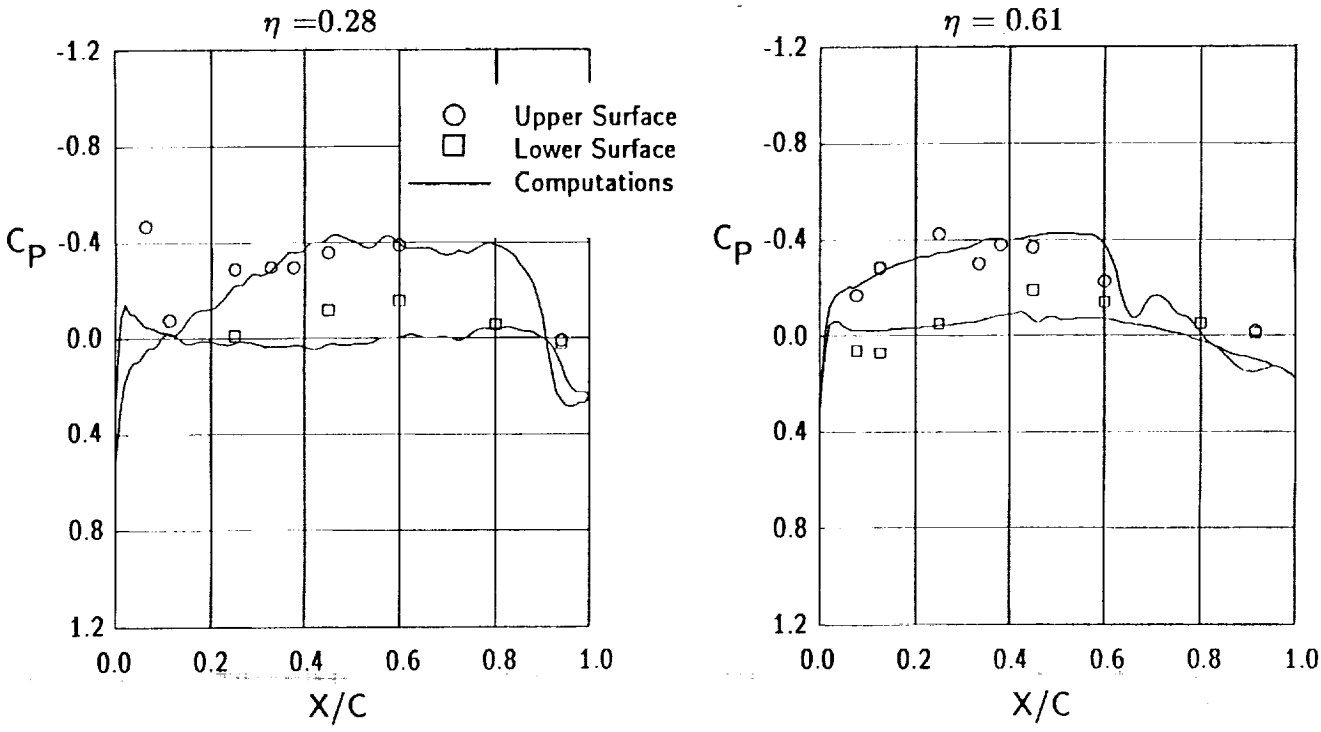

b) Canard

Figure 16 - Comparison of computational results and flight test data - M=0.91, $\alpha = 4.2°$